*Geotechnical Aspects of Underground Construction in Soft Ground – Yoo, Park, Kim & Ban (Eds)*


# Effect of repeated shear deformation on twin tunneling – model test and finite element analysis

H.M. Shahin & S. Kuroi
*Nagoya Institute of Technology, Nagoya, Japan*

T. Nakai
*Geo-Research Institute, Nagoya Branch, Nagoya, Japan*

ABSTRACT: Number of parallel tunnels is increasing day by day to meet the demand of modernization. During earthquake soil is experienced with shear deformation due to ground excitation. Therefore, it is necessary to check the behavior of twin tunneling during and after earthquake for a safe and secured tunnel construction. In this research, behavior of twin tunnels during the application of repeated shear deformation has been investigated with a new tunnel device. The device consists of two model tunnels which are free to move along with the soils of the ground. Here, several tests are conducted changing the position of following tunnel. In the tests, repeated shear deformation is applied in the ground through the application of horizontal inertial force after the completion of twin tunnels excavation. Earth pressure of the tunnels are measured during the application of shear deformation. The corresponding non-linear finite element analyses are also conducted using FEMtij-2D program where elastoplastic subloading $t_{ij}$ model is used as a constitutive model of soil. From the model tests and numerical simulations it is found that the earth pressure around the tunnels changes significantly according to the direction of the repeated shear.

## 1 INTRODUCTION

To meet the demand of modernization tunneling is increasing day by day all over the world which emphasizes the necessity of a safe and secured tunnel construction. It is commonly said that there is little influence of seismic motion on tunnel structures. The superstructures such as bridge, buildings significantly vibrate as the resonance of the superstructures itself dominate which occurs along with the inertial force during seismic motion. However, the resonance of the tunnel is less significant as the inertial force acting on the tunnel is smaller than that of the surrounding ground and the tunnel vibrates following the displacement and deformation of the ground. Furthermore, since the shield tunnel is built in the subterranean deeper place which is not experienced with significant deformation during earthquake, and as a circular tunnel section is usually strong against deformation, it is thought that a tunnel structure is not almost experienced the effect of earthquake. However, it is revealed in an investigation, reported by Japan Society of Civil Engineers (1997), cracks occurred to secondary lining concrete in a shield tunnel during the Great Hanshin-Awaji Earthquake. During earthquake as soil is experienced with shear deformation due to ground acceleration and non-uniform sectional force develops at that places where there are sudden changes in ground conditions and at the conjugation of soil-structure, it requires sufficient investigation in the design stage. In this research, a new tunnel device (Shahin et al. 2013) has been developed to investigate fundamental dynamic action on the tunnel in the case of earthquake applying repeated shear deformation. The corresponding finite element analyses are conducted with FEMtij-2D program where elastoplastic subloading $t_{ij}$ model (Nakai & Hinokio 2004) is used as a constitutive model of soil. This model can describe typical stress deformation and strength characteristics of soils such as the influence of intermediate principal stress, the influence of stress path dependency of plastic flow and the influence of density and/or confining pressure.

## 2 DESCRIPTIONS OF MODEL TESTS AND NUMERICAL SIMULATIONS

### 2.1 *Layout of model tests*

Figure 1 shows a tunnel apparatus after the modification of the previous tunnel device (Shahin et al. 2013). In the device, the excavation part can be moved freely upward and downward, and left and right without friction by a bearing and a horizontal slider attached in the device. The weight of the entire model tunnel is balanced with a counter weight which is acted through a fixed pulley set at the top of the device. As a result,

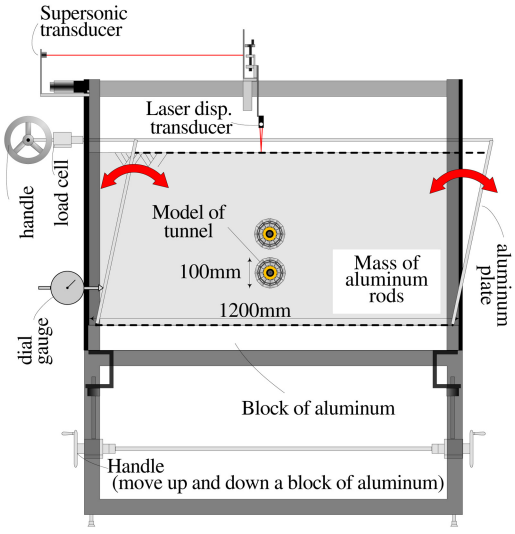


Figure 1. Schematic diagram of tunnel device.

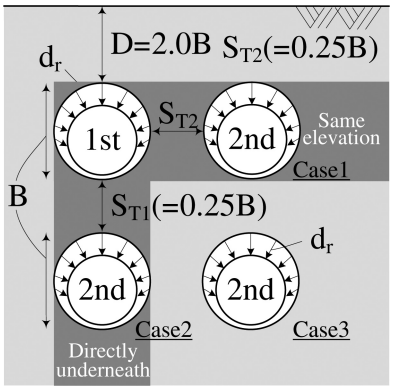


Figure 2. Different positions of tunnels.

the tunnel excavation can be simulated by leaving it to an equilibrium condition of the vertical and lateral earth pressures controlling the amount of shrinkage of the tunnel diameter. The total diameter of the tunnel is 10 cm and the device consists of a shim at the center of the tunnel surrounded with 12 segments having load cells to measure earth pressure acting on the tunnel. The length of the apparatus is 120 cm, and the tunnel devices are set up somewhat middle of the apparatus to avoid boundary effect to the results of the experiments. For simulating single tunnel only one tunnel device is set up in the apparatus, and for getting the interaction effect of twin tunnels two tunnel devices are set up during experiment. The apparatus consists an aluminum block which can be moved in the vertical direction. The dimension of the apparatus is chosen with a scale of 1:100 between the model and prototype scales. Therefore, the diameter of 10 cm corresponds to the tunnel of 10m in the real ground condition. Mass of aluminum rods, having diameters of 1.6 and 3.0 mm mixed in a ratio of 3:2 in weight, is used as ground material. The unit weight of the aluminum rods mass is 20.4 kN/m$^3$, and the length is 50 mm. The properties of the ground mass consisting aluminum rods are similar to the properties of dense sand (Shahin et al. 2013). The initial ground is made in such a way that the earth pressure around the tunnel becomes similar to the earth pressure at rest adjusting the block of aluminum set at the bottom of the apparatus. The tunnel excavation is simulated by controlling the shrinkage of the tunnel device.

In the new apparatus, the frames of the both sides are set with hinges at the bottom end to allow the ground movement in the horizontal direction. The upper parts of the both side's frames are connected with an aluminum bar to apply the same shear deformation at both left and right sides of the ground. The dotted lines in Figure 1 show the direction of shear strain in a particular direction which can be achieved with the new apparatus. A load cell is attached to the left side frame which is connected with a handle to apply inertial force in the ground. The horizontal displacement of the ground is measured with a dial gauge which is attached to the left side frame from which the magnitude of the average shear strain ($\gamma$) is obtained. In the experiment, at first tunnel excavation is simulated by shrinking the tunnel device with 4 mm, the shrinkage of the tunnel is represented with $d_r$. In twin tunneling, three tests patterns are considered – (a) Case 1: the following tunnel is excavated in the same elevation of the preceding tunnel, (b) Case 2: the following tunnel is excavated directly underneath of the preceding tunnel, and (c) Case 3: the following tunnel is excavated diagonally underneath of the preceding tunnel. Figure 2 illustrates the positions of the twin tunneling. The vertical distance between the twin tunnels is represented with $S_{T1}$ and the horizontal distance between the twin tunnels is represented with $S_{T2}$. In this paper, $S_{T1} = S_{T2} = 0.25$. After completion of the tunnel excavation, the initial ground is taken ($\gamma = 0$) into consideration in this research. The shear strains are applied in the ground up to 4 cycles by applying inertial force. Here, the value of inertial force is chosen from the horizontal seismic coefficient ($k_h$) of 0.4. Where, the value of horizontal seismic coefficient ($k_h$) is the load per unit weight, i.e., $k_h = F_h/W$; $F_h$ is the inertial force and $W$ is the weight of the whole ground. The tests have been conducted for a fixed overburden ratio, $D/B = 2.0$, where $D$ is the depth from the ground surface (for twin tunneling it is the upper tunnel) to the top of the tunnel and $B$ (=10 cm) is the width of the tunnel.

## 2.2 *Layout of numerical analyses*

The numerical analyses are performed with the same scale of the model tests. Figure 3 shows a typical mesh used in the finite element analyses. Simulations are carried out considering the same scale and conditions of the model tests. The frames at both sides and the top are modelled with beam element. The

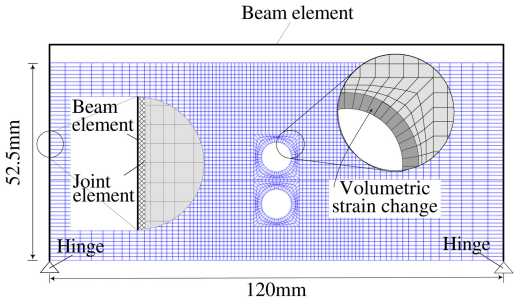


Figure 3. Typical finite element mesh.

Table 1. Parameters of mass of aluminum rod.

| Parameter | Value |
|---|---|
| $\lambda$ | 0.0080 |
| $\kappa$ | 0.0040 |
| $N$ ($e_{NC}$ at $p = 98$ kPa & $q = 0$ kPa) | 0.30 |
| $R_{CS} = (\sigma_1/\sigma_3)_{CS(comp.)}$ | 1.80 |
| $\beta$ | 1.20 |
| $\nu_e$ | 0.20 |
| a | 1300 |

interface between the frames and the ground is modelled with elastoplastic joint element (Nakai 2005). Isoparametric 4-noded elements are used in the mesh. The bending moments at the bottom most nodes of the frame are assigned to zero for imposing hinge boundary of the beam elements. Smooth boundary conditions are imposed at both sides of the mesh, and the bottom face is kept fixed. To simulate the tunnel excavation, compressive volumetric strain in the tunnel elements is applied which corresponds the amount of radial shrinkage of the tunnel. This is an important simulation technique to consider the free movements of the tunnel. After the simulation of tunnel excavation, repeated shear deformation is imposed into the ground applying cyclic loading at the top most node of the left boundary.

Two-dimensional finite element analyses are carried out with FEMtij-2D using the subloading $t_{ij}$ model (Nakai & Hinokio 2004). Model parameters for the aluminum rod mass are shown in Table 1. The parameters are fundamentally the same as those of the Cam clay model except the parameter a, which is responsible for the influence of density and confining pressure. The parameter $\beta$ represents the shape of yield surface. The parameters can easily be obtained from traditional laboratory tests. Figure 4 shows the results of the biaxial tests for the mass of aluminum rods used in the model tests. From the stress-strain behavior of the element tests simulated with subloading $t_{ij}$ model, it is noticed that this model can express the dependency of stiffness, strength and dilatancy on the density as well as on the confining pressure. It is clear that the strength and deformation behavior are very similar to those of dense sand. The dotted lines represent the numerical results for a confining pressure of

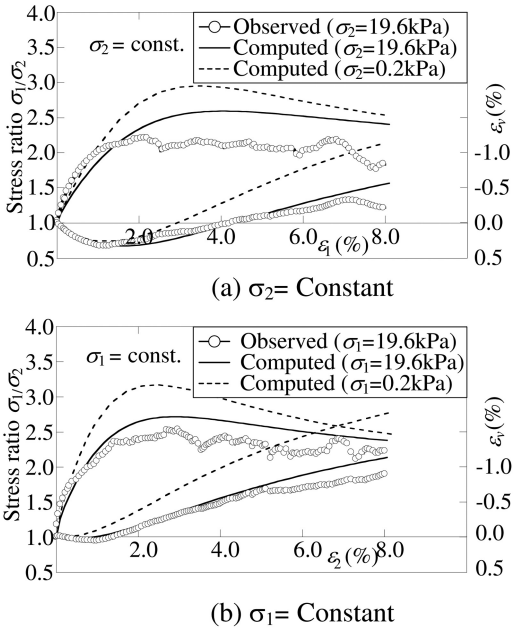


Figure 4. Stress-strain-dilatancy relation of aluminum rods mass.

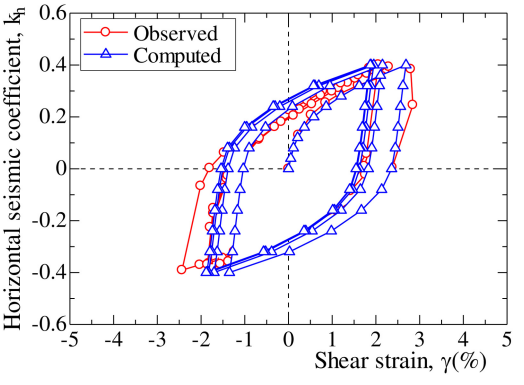


Figure 5. Relation of horizontal seismic coefficient with shear strain.

1/100 times the confining pressure in the experiments. The initial stress levels of the ground are calculated by applying the body forces due to the self-weight ($\gamma = 20.4$ kN/m$^3$), starting from a negligible confining pressure ($p_0 = 9.8 \times 10^{-6}$ kPa) and an initial void ratio of $e = 0.35$. After self-weight consolidation, the void ratio of the ground is in between 0.28 to 0.30. The value of $K_0$, derived from the simulation of the self-weight consolidation is in between 0.70 and 0.73.

## 3 RESULTS AND DISCUSSIONS

### 3.1 *Single tunnel excavation*

Figure 5 represents observed and computed relation of the horizontal seismic coefficient with shear strain of

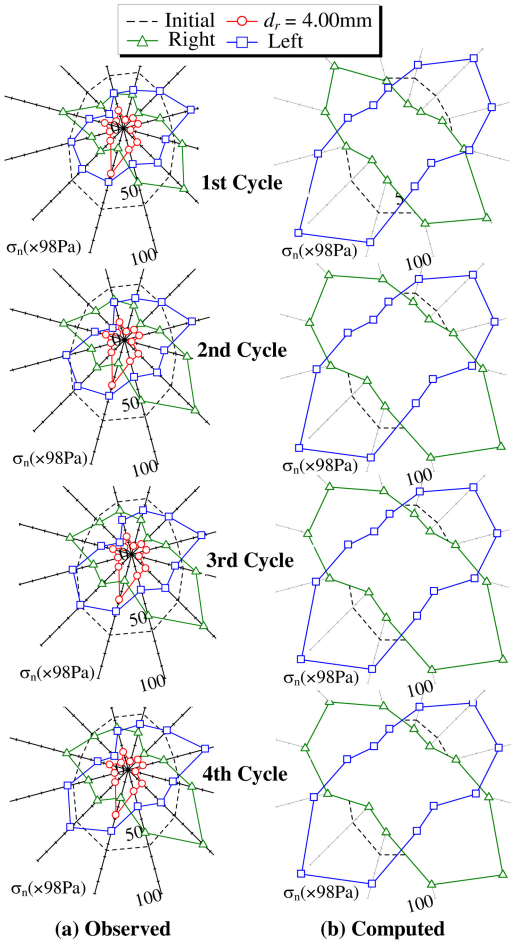


Figure 6. Distribution of earth pressure around tunnel: single tunnel.

the tunnel ground for cyclic loading. It is seen that the after few cycles of loading the stiffness of the ground material becomes constant. The numerical analyses perfectly capture the stiffness of the model ground.

Figure 6 shows the observed and computed earth pressure distributions around tunnel periphery. The plots are drawn in the 12 axes corresponding to the radial direction of the 12 load cells towards the center of the model tunnel. The figures represent the value of earth pressure for the first to the fourth cycles of loading after applying maximum loadings to the right ($k_h = 0.4$) and left ($k_h = -0.4$) directions. The figure also shows the earth pressure at initial ground and after the amount of shrinkage $d_r = 4$ mm (tunnel excavation). It is seen that for the excavation of the tunnel earth pressure decreases around this tunnel due to the arching effect, the same way as the results of the references (Murayama & Matsuoka 1971, Shahin et al. 2004, 2011, Sung et al. 2006). It is seen in the results of the 1st cycle, the earth pressure increases significantly at the right shoulder and its opposite side due

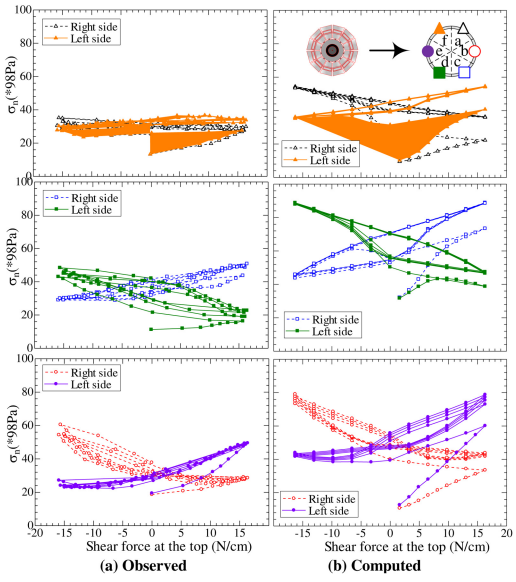


Figure 7. History of earth pressure around tunnels.

to the application of shear strain when $k_h = 0.4$. When $k_h = -0.4$, i.e. the ground is moved to the left direction, earth pressure decreases at the right shoulder and its opposite side, and at the same time earth pressure increases at the left shoulder and its opposite side. The results of the other cycles show the repetition of increase and decrease of the earth pressure at the right and left shoulders and their opposite sides the same way as the 1st cycle. Though the numerical simulation produces larger value of the earth pressure compare to the model test, t, the mode and the tendency of the increase and decrease in earth pressure are similar to that of the model test.

Figure 7 illustrates the history of the change in earth pressure where the surrounding earth pressure of the tunnel is divided into six domains. The results represent the change of earth pressure of each domain for the shear deformation of 4 cycles. The results confirm the repetition of increase and decrease in earth pressures of each domain during the application of repeated shear to the right and left directions.

### 3.2 *Twin tunnel excavation*

Figure 8 represents the observed earth pressure distributions around the peripheries of both preceding and following tunnels. Figure 9 shows the results of the finite element analyses for the same. The plots are drawn in the 12 axes corresponding to the radial direction of the 12 load cells towards the center of the model tunnel the same way as the single tunnel excavation demonstrated in Fig. 6. The figures represent the value of earth pressure at the end of each cycle of loading. Each figure contains the results of four cycles of loadings together with the results at the end of both tunnel excavation representing with circular

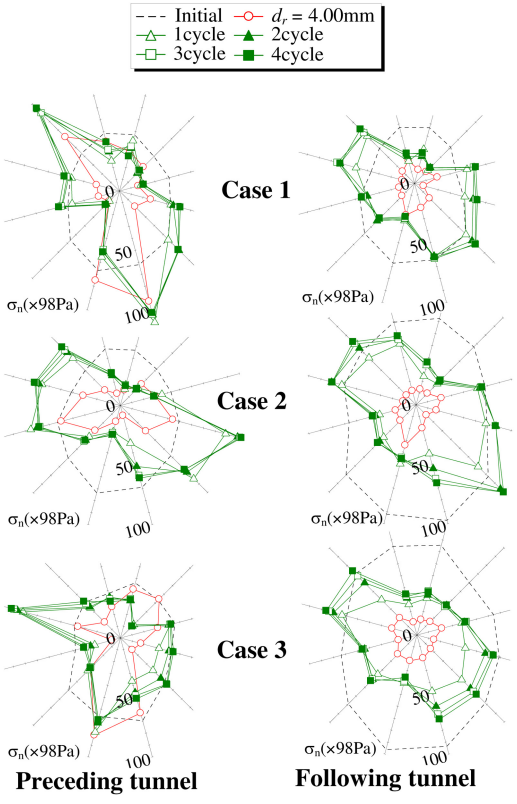


Figure 8. Observed distribution of earth pressure around both tunnels: twin tunneling.

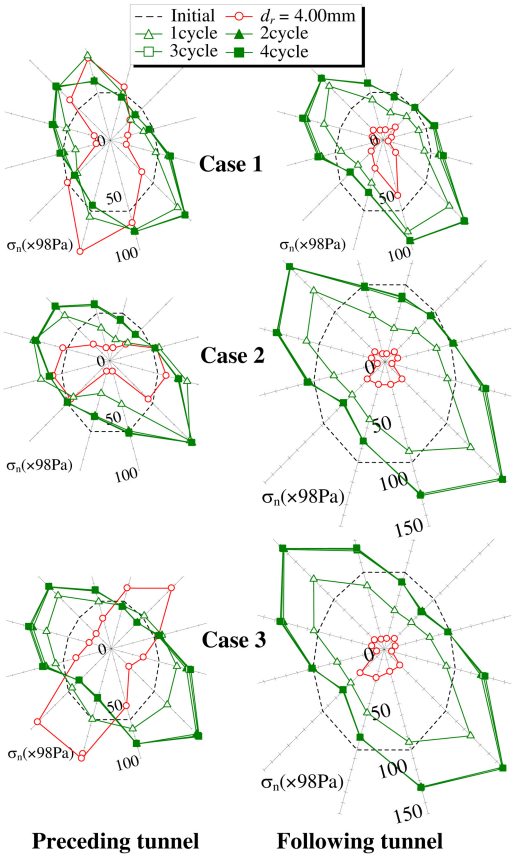


Figure 9. Computed distribution of earth pressure around both tunnels: twin tunneling.

marks ($d_r = 4$ mm). It is seen in the results of the preceding tunnel that earth pressure changes (increases and decreases) due to the excavation of the nearby following tunnel. The changing pattern of earth pressure varies on the location of the following tunnel which agrees with the results of the previous research (Shahin et al. 2012). The earth pressure of the existing tunnel increases at the vertical direction to the nearby following tunnel. As mentioned in the section of the layout of experiments, Case 1 represents the case where following tunnel is located in the same elevation, in Case 2 the following tunnel is located vertically download direction, and for Case 3 it is in the diagonally downward direction.

It is seen that due to the effect of repeated shear deformation ($k_h = -0.4$) the earth pressure increases significantly at different positions of the tunnel periphery depending on the distributions of earth pressure at the moment immediately before applying the inertial force. For Case 1, a significant increase of earth pressure is seen at the left shoulder (near crown) and its opposite side (near invert) due to the application of repeated shear deformation. For Case 2, the increase in earth pressure is significant near the spring line of the preceding tunnel. For the all cases, there is not much differences in the earth pressure from the first cycle of loading at the preceding tunnel. In contrast, from the second cycle of loading the earth pressures at the following tunnel are almost same. It is also revealed that the shape of the earth pressure distributions is a bit different between the preceding and the following tunnels for the same case. Therefore, it necessary to consider the interaction effect of twin tunneling during the consideration of seismic effect for a safe tunnel construction. Though the numerical simulation produces a larger value of the earth pressure compare to the model test, the mode and the tendency of the increase and decrease in earth pressure are similar to that of the model test the same way as the results of the single tunnel. Interface element between the ground materials and the tunnel are not considered in the analyses which might be the cause of the over prediction of the results.

## 4 CONCLUSIONS

From the model tests and numerical simulations it is found that the earth pressure around the tunnel increases and decreases significantly according to the directions of the repeated shear. This is because the direction at which the arching effect is developed

changes with the loading directions. With the repeated loading the stiffness increases as a mechanical characteristic of the ground material, hence the earth pressure around the tunnel increases to some extent. In the case of twin tunneling, mode of the earth pressure distributions varies on the location of the following tunnel excavation due to the effect of cyclic loading. Therefore, it is necessary to consider such important factors in a tunnel design to withstand from the seismic motion during earthquake, and the interaction of parallel tunnels should be predicted carefully for the twin tunneling. The numerical analyses capture the distributions of earth pressure of the tunnel in different cases.

## ACKNOWLEDGEMENTS

This study is supported financially in part by the Grant-in-Aid for Young Scientists (B) (24760378, Hossain Md. Shahin) from Ministry of Education, Science and Culture in Japan and the research grant from the Advanced Construction Technology Center.

## REFERENCES

Adachi, T., Tamura, T., Kimura, M. & Aramaki, S. 1994. Earth pressure distribution in trap door tests. *Proc. of 29th Japan National Conference of SMFE*, Vol. 3: 1989–1992, (in Japanese).

Japan Society of Civil Engineers, 1997. The Great Hanshin-Awaji Earthquake investigation report, (in Japanese).

Murayama, S. & Matsuoka, H. 1971. Earth pressure on tunnels in sandy ground. *Proc. of Japan Society of Civil Engineers*, 187: 95–108, (in Japanese).

Nakai, T. 1985. Finite element computations for active and passive earth pressure problems of retaining wall. *Soils and Foundations*, 25(3): 98–112.

Nakai, T. & Hinokio T. 2004. A simple elastoplastic model for normally and over consolidated soils with unified material parameters. *Soils and Foundations*, 44(2): 53–70.

Shahin, H. M., Nakai, T., Hinokio, M., Kurimoto, T., & Sada, T. 2004. Influence of surface loads and construction sequence on ground response due to tunneling. *Soils and Foundation*, 44(2): 71–84.

Shahin, H. M., Nakai, T., Zhang, F., Kikumoto, M. & Nakahara E. 2011. Behavior of ground and response of existing foundation due to tunneling. *Soils and Foundations*,
51(3): 395–409.

Shahin, H. M., Nakai, T. & Kuroi, S. 2013. Tunnel behavior subjected to repeated shear deformation – model test and finite element analysis, *3rd International Conference on Computational Methods in Tunnelling and Subsurface Engineering*, Germany, April, pp. 283–292.

Shahin, H. M., Nakai, T. & Iwata T. 2012. Model tests and numerical simulation on tunneling in urban area. *Proc. of the 6th New Frontiers in Computational Geotechnics,* Japan, May, pp. 87–92.

Sung, E., Shahin, H. M., Nakai, T., Hinokio, M. & Yamamoto, M 2006. Ground behavior due to tunnel excavation with existing foundation. *Soils & Foundations*, 46(2): 189–207.